Influence of the surface morphology on the cyclic deformation behavior of HSD® 600 steel

Matthias W. Klein[1*], *Marek* Smaga[1], and *Tilmann* Beck[1]

[1]Institute of Materials Science and Engineering, TUK , 67663 Kaiserslautern, Germany

Abstract. The presented research work investigates the fatigue properties in the low cycle fatigue (LCF) regime of the high manganese metastable austenitic High Strength and Ductility (HSD®) 600 TWIP steel dependent on its surface morphology. The steel features, according to its chemical composition following the alloying concept Mn-Al-Si-C and heat treatment, a fully austenitic microstructure that shows deformation induced twinning at ambient temperature. Due to this microstructural deformation mechanism, HSD® 600 steel has an outstanding combination of strength and formability. Besides monotonic deformation behavior, characterized by tensile tests, cyclic deformation behavior was investigated with varying the surface morphology of fatigue specimens. In order to create different surface morphologies, flat fatigue specimens were excised from larger sheets by waterjet-cutting. Depending on the surface morphology, further climb milling or up-climb milling in the gauge length was performed. The three investigated morphologies (as-received with rolling skin, climb milled and up-climb milled) differed in roughness, initial residual stresses and initial phase compositions. For all variants, total strain controlled fatigue tests with stepwise increasing load amplitudes as well as total strain controlled single step tests were performed in the low cycle fatigue regime with a load ratio of R_ε = -1 and a frequency of f = 0.2 Hz. Beside stress-strain hystereses, the changes in temperature ΔT and the magnetic properties ξ were measured. The magnetic properties directly correlate with the transformation from paramagnetic γ-austenite to ferromagnetic α'-martensite. The cyclic deformation behavior of the HSD® 600 steel in the LCF regime was characterized by cyclic softening until fracture at low total strain amplitudes but changed with increasing total strain amplitudes into initial cyclic hardening followed by cyclic softening. This initial cyclic hardening became more pronounced when the total strain amplitude increased. Furthermore, single step tests at lower total strain amplitudes showed a saturation state before fracture. A comparison between the monotonic and cyclic deformation behavior showed a significant difference of the stress levels at the same amounts of plastic deformation respectively. Nevertheless, the different surface morphologies led to different lifetimes at high total strain amplitudes but to similar lifetimes at lower total strain amplitudes.

1 Introduction

TWinning Induced Plasticity (TWIP) steels with the alloying concept Mn-Al-Si-C offer an outstanding combination of strength and formability due to deformation induced microstructural mechanisms like twinning [1]. These properties are needed for new design concepts for energy absorbing applications such as crash resistant components in the automotive industry or deep drawing of sheet materials [1].

TWIP steels typically have an austenitic microstructure at ambient temperature. The TWIP mechanism is characterized by the formation of deformation twins. These twins represent strong barriers for mobile dislocations and cannot be circumvented, and therefore further dislocation pile-up occurs. This ongoing process is called the dynamic Hall-Petch effect [2, 3]. The activation of deformation induced mechanisms depends on the Stacking Fault Energy (SFE) and consequently on the chemical composition of the material. High manganese steels with additions of aluminum and silicon achieve SFE < 60 mJ/m² [4].

Several investigations have characterized the cyclic deformation behavior of high manganese TWIP steels. Hamada et al. [5] showed that a short period of cyclic hardening is followed by cyclic softening and a saturation state until fracture. In addition Shao et al. [6] made similar observations and reported further that in the LCF regime the amount of the initial cyclic hardening increases with increasing total strain amplitude. At low and moderate total strain amplitudes ($\varepsilon_{a,t}$ < 1.0 %) the degree of cyclic softening is enhanced. Thus, the authors observed deformation induced twins beside the formation of dislocation cells with relatively small size. Both phenomena became more pronounced

* Corresponding author: mwklein@mv.uni-kl.de

by increasing the total strain amplitude. Moreover, Guo et al. [7] investigated the cyclic deformation behavior with varied total strain amplitudes from 0.2 % until 1.0 % of a high manganese TWIP steel. They showed that within the first 5 percent of lifetime, cyclic hardening occurs but the subsequent behavior is strongly dependent on the applied total strain amplitude. At total strain amplitudes of 1.0 % to 0.6 % the initial cyclic hardening merged into cyclic softening until fracture: At lower total strain amplitudes of 0.4 % and 0.3 % cyclic saturation was observed before fracture and at a total strain amplitude of 0.2 % the initial cyclic hardening remained until fracture. Furthermore, the cyclic yield strength, determined by stress-strain hystereses, exceeded the monotonic yield strength.

It is well known, that the surface morphology, consisting of residual stresses, phase composition and roughness, significantly influences fatigue properties by influencing the initial fatigue damage at the surface [8]. Therefore, in metastable austenitic steels, there are efforts to modify surface layers for improving fatigue lifetime by inducing compressive residual stresses, increasing the dislocation density, inducing of nanostructures and phase transformation from paramagnetic γ-austenite to paramagnetic ε-martensite and/or ferromagnetic α'-martensite [8, 9]. In addition, the development of surface morphologies during fatigue loading is also important. For example, relaxation and redistribution of residual stresses due to cyclic loading can be observed [10]. In the literature, there are many investigations about the influence of morphology on the fatigue properties of austenitic stainless steels with the alloying concept Fe-Cr-Ni-C, but hardly any on high manganese austenitic TWIP steels. Therefore, the aim of this investigation is to characterize the influence on fatigue properties in the LCF regime of a high manganese TWIP steel with different surface morphologies, created by different machining parameters. The initial surface morphologies were characterized by SEM, XRD and confocal microscopy methods before push-pull testing until fracture in the LCF regime.

2 Material and experimental setup

2.1 HSD® 600 steel

The investigated material was the HSD® 600 steel, delivered as flat sheets with a thickness of 5 mm in hot rolled state. The chemical composition is given in table 1.

Table 1. Chemical composition in weight %

Element	C	Mn	Al	Si
weight %	0.36	15.29	1.80	2.29

The material has a mean grain size of about 20 µm, determined including annealing twins. Note, that the grain size varies from relatively large grains up to 40 µm to small grains of about 10 µm (Fig. 1 a)). EBSD analysis shows no preferred grain orientation in this material. In addition, the hardness is 301±13, determined by Vickers indentation HV10.

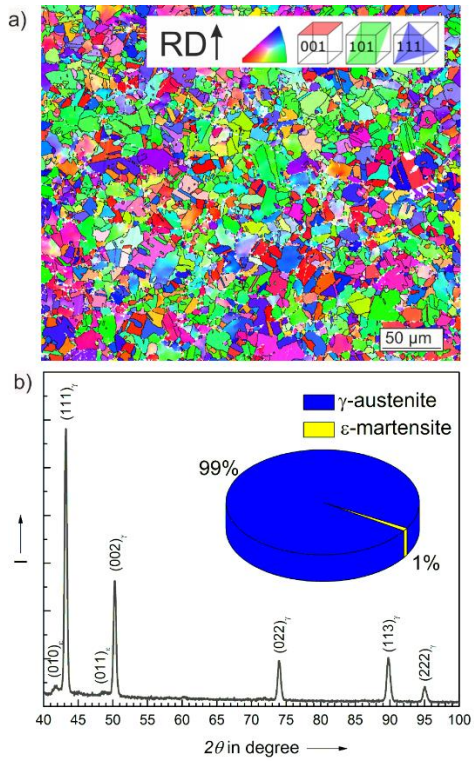

Fig. 1. Microstructure in longitudinal section of HSD® 600 steel at the initial state a) grain orientation in rolling direction (RD); b) x-ray diffraction pattern and phase composition

The initial state is nearly fully austenitic. Nevertheless, a small volume fraction of 1 wt % ε-martensite can be found by x-ray diffraction using the Rietveldt method [3] after wet grinding up to 1200 grit followed by electrolytic polishing (Fig 1 b)).

2.2 Experimental setup

The sin²ψ-method was used for determining residual stresses while x-ray diffraction patterns were measured with the PANalytical diffractometers MRD Pro and Empyrean operating at 40 kV and 40 mA using $CuK_{\alpha 1}$ radiation and a spot size of 3 x 3 mm. The Rietveldt-method was used for quantitative phase analysis. SEM investigations were carried out with a Quanta 600, FEI with an EBSD module hkl 5, Oxford instruments. The phase transformation from γ-austenite to α'-martensite during cyclic loading was measured in-situ using a magnetic sensor Feritscope® MP30E, Helmut Fischer. The ferromagnetic fraction (ξ) of the material is given in FE-% and correlates directly with the volume fraction of α'-martensite. Topographies were characterized by confocal microscopy using µSoft explorer, µSurf.

Monotonic loading of flat specimens was performed on the Zwick Z250 tensile test machine with a maximum force of 250 kN. The strain rate was $\dot{\varepsilon} = 2.5 \times 10^{-4}\ s^{-1}$

reaching the 0.2 % yield stress until $R_{p0.2}$ and was then increased to 6.7 x10^{-3} s^{-1}. The strain in loading direction was measured by an electromechanical extensometer, while strain in transverse direction was measured optically by a video extensometer.

To characterize the cyclic deformation behavior, single step tests and strain increase tests with flat fatigue specimens with a gauge length of 8 mm were performed. The tests were total strain controlled at ambient temperature (AT), at a frequency of f = 0.2 Hz and load ratio of R_ε = -1 in the LCF regime on a MTS 810 servohydraulic testing system with a maximum push-pull force of 100 kN. The load-time function was triangular. Besides stress-strain hystereses, changes in temperature T were calculated by equation (1) from temperatures measured by three thermocouples (Fig. 2).

$$\Delta T = T_1 - \frac{1}{2}(T_2+T_3) \quad (1)$$

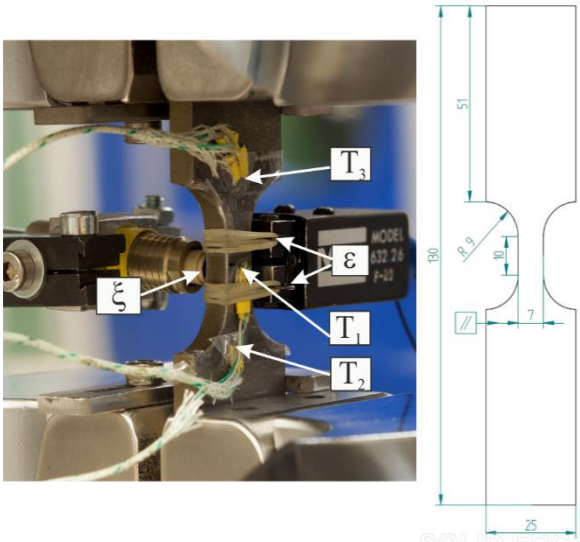

Fig. 2. Experimental setup for fatigue testing and specimen geometry (sample)

Due to machining, the specimens vary in thickness. Therefore, the gauge length of each specimen was measured before testing. Specimens with rolling skin morphology (i.e. from as-received sheets) had a thickness of 5 mm, while specimens with the climb milled and up-climb milled morphologies were 4.6 mm thick (see 2.3).

2.3 Investigated morphologies

Flat specimens were excised transverse to the rolling direction by waterjet-cutting and depending on the investigated surface morphology, further machining was performed before cyclic loading. Three different surface morphologies were investigated: as-received with a so called rolling skin of about 30-40 µm thickness formed during the manufacturing process (M_{RS}), after climb milling the gauge length (M_{CM}) and after up-climb milling the gauge length (M_{UCM}) (Fig. 3). For the machined morphologies M_{CM} and M_{UCM} the machining parameters, given in table 2, were identical, despite the rotation direction of the milling tool.

Table 2. Machining parameters for morphologies M_{CM} and M_{UCM}

tool coating	f_z	n	n_z
AlTiN	0.025	5091	4

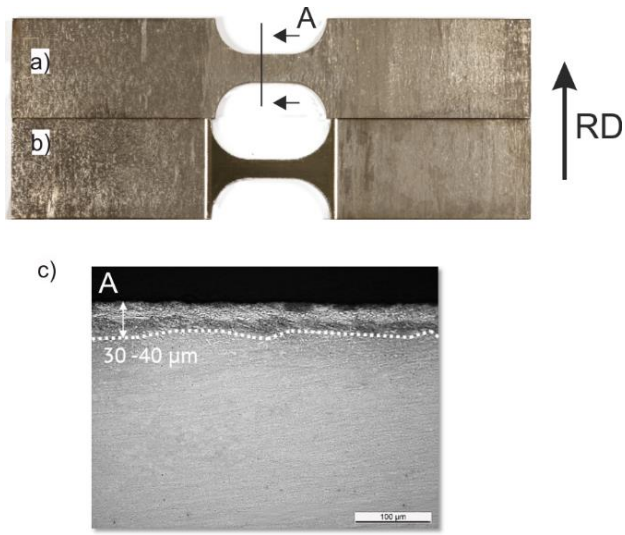

Fig. 3. Sample surface morphologies: a) as-received with rolling skin (M_{RS}); b) climb-milled (M_{CM}); c) cross section of M_{RS} with the thickness of the rolling skin

These four morphologies have different properties concerning roughness, initial residual stresses, phase composition and topography.

The topographies of the morphologies were quantified by the value R_z (Fig. 4). R_z is defined as the average distance between the highest peak and the lowest valley of the sampling length. The morphology M_{RS} showed the highest value of R_z due to no further machining after the specimens were cut. The climb milled specimen showed smoother surfaces than the up-climb milled surfaces, but on both surfaces the traces of the milling tool were visible.

Table 3. Roughness of the investigated surface morphologies

Morphology	M_{RS}	M_{CM}	M_{UCM}
R_z in µm	6.17	0.75	1.18

Due to machining process, the unevenness of the morphologies M_{CM} and M_{UCM} repeated periodically while the surface of M_{RS} was irregular.

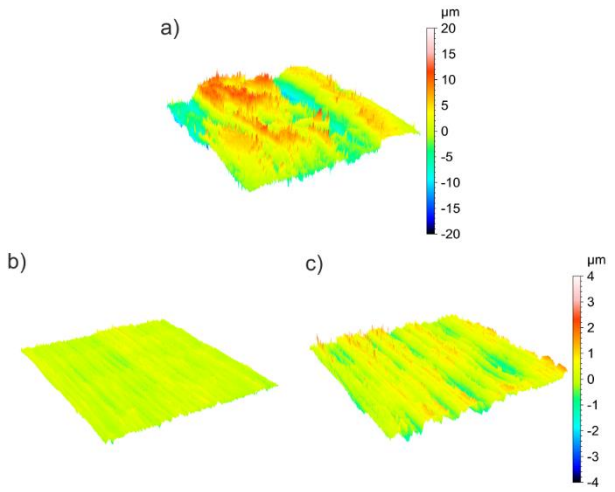

Fig. 4. Topographies of the investigated morphologies a) as-received with rolling skin (M_{RS}); b) climb-milled (M_{CM}); c) up-climb milled (M_{UCM})

Besides the roughness, the morphologies showed wide disparities in phase compositions and initial residual stresses (Fig. 5). A significant amount of α'-martensite was present on the surface of the morphology M_{RS}. The absence of α'-martensite after metallographic polishing indicated (Fig. 1), that this phase was present in the surface layer induced by the manufacturing process. The morphologies M_{CM} and M_{UCM} were austenitic, despite a small amount of ε-martensite of approximately 4 wt % in M_{CM} and 1 wt % in M_{UCM}.

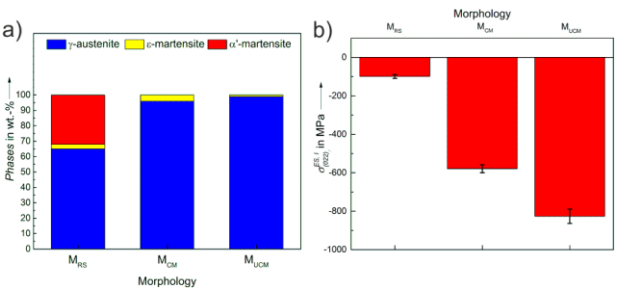

Fig. 5. Surface morphologies before loading: a) phase compositions; b) initial residual stresses

Each morphology showed compressive residual stress in the loading direction before loading, but the amount varied strongly. The morphology M_{UCM} showed the highest value of -800 MPa while morphology M_{CM} had lower values of -600 MPa. The milling process induced these compressive stresses. Due to no further machining after waterjet-cutting, the morphology M_{RS} showed significantly lower values of residual compressive stress of -100 MPa.

3 Results

3.1 Monotonic deformation behavior

For M_{RS} specimens, the monotonic deformation behavior was investigated transversely and longitudinally to the rolling direction (RD) (Fig. 6). The mechanical properties in both directions are given in table 2.

Table 4. Quasi-static properties longitudinal and transverse to rolling direction

	Longitudinal	Transverse
R_m in MPa	1028±10	1044±4
$R_{p0.2}$ in MPa	607±21	621±5
Elongation in %	53±2	51±1
Young's Modulus in GPa	169±7	180±1
Poisson's ratio	0.24±0.04	0.24±0.04

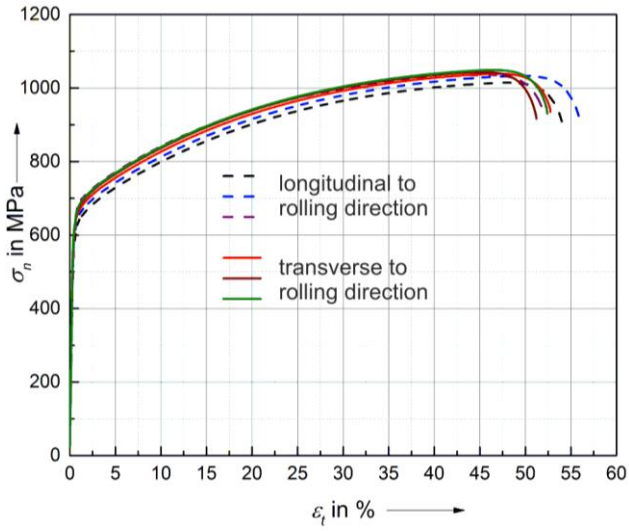

Fig. 6. Monotonic stress-strain curves of specimen taken longitudinally and transversely to rolling direction

The stress-strain curves showed a similar behavior of the material in both directions. Furthermore, the monotonic deformation behavior was characterized by a large amount of plastic deformation up to an elongation of 50 %, while tensile strengths of about 1000 MPa were reached. This demonstrates the aforementioned combination of strength and formability, which is typical for high manganese TWIP steels. No pronounced yield limit was noticeable.

3.2 Strain increase tests (SIT)

To characterize the cyclic deformation behavior at different total strain amplitudes, strain increase tests (SIT) were performed at specimens with the three different surface morphologies (Fig. 7). The total strain amplitude started at $\varepsilon_{a,t}$ = 0.2 % and was increased each 100 cycles by $\Delta\varepsilon_{a,t}$ = 0.05 %. For all morphologies in the first step, no cyclic hardening or softening was noticeable in the stress amplitude σ_a. From the second step, cyclic softening occurred, determined by decreasing stress amplitude σ_a. However, with increasing total strain amplitude $\varepsilon_{a,t}$ cyclic softening decreased until within the first cycles of one step cyclic hardening occurred (enlarged details of Fig. 7). Thus, the cyclic deformation behavior of all three morphologies depended on the applied total strain amplitude $\varepsilon_{a,t}$. This behavior was also noticeable in the changes in temperature because of its correlation with the area of stress-strain hystereses [11]. The temperature increased due to larger stress-strain hystereses while cyclic softening occurred in the first steps, and decreased in later steps while cyclic hardening was occurring.

Even though the behavior of the materials with three different surface morphologies is comparable in general, the surface morphologies led to different results of the strain increase tests. The specimens with morphology M_{RS} showed phase transformation from γ-austenite to α'-martensite, which was noticeable in changes to their magnetic properties while testing. The milled morphologies M_{CM} and M_{UCM} remained fully austenitic and no changes in magnetic properties occurred. Thus, the rolling skin of M_{RS} is metastable depending on its phases. Nevertheless, the morphology M_{RS} led to the lowest lifetime due to its significantly higher roughness.

The morphology M_{UCM} led to the highest lifetime, although the same applied total strain amplitudes led to lower stress amplitudes at the morphology M_{CM}. Note, that the described phenomena occurred significantly below the yield strength $R_{p0.2}$ which clearly differed from the results shown by the literature for high manganese austenites, and even for austenitic stainless steels [6, 7].

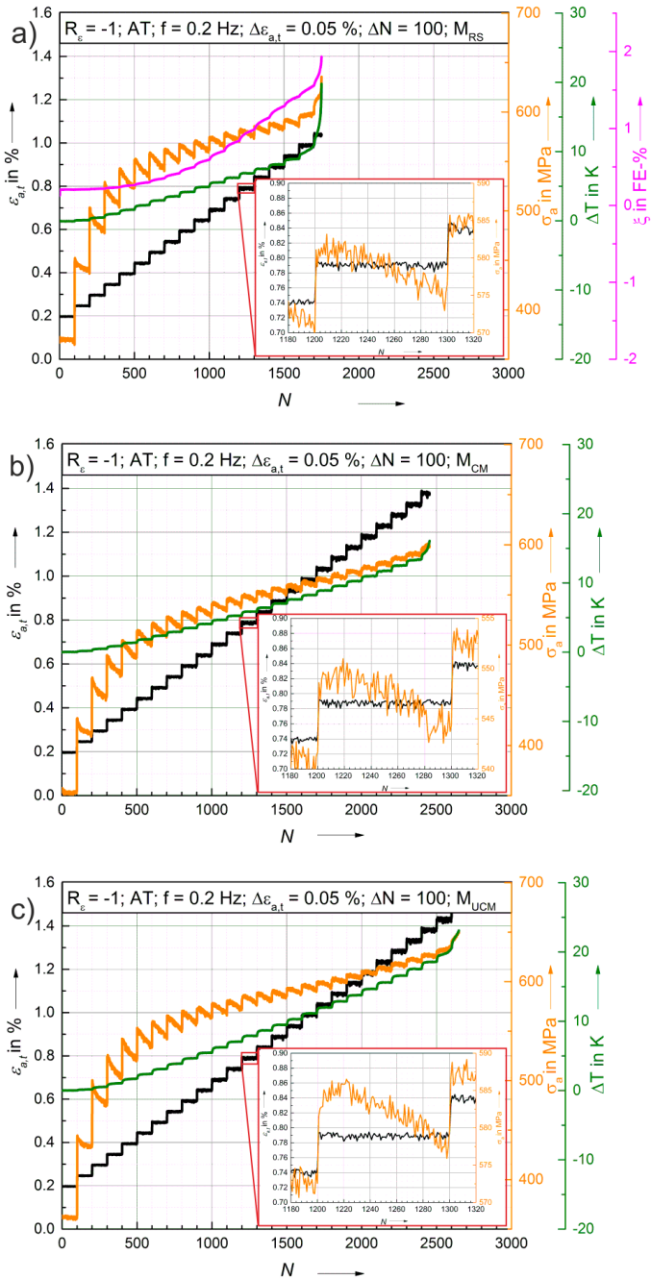

Fig. 7. Development of stress amplitude and temperature versus number of load cycles in strain increase tests (SIT): a) as-received with rolling skin with development of α'-martensite (M_{RS}); b) climb-milled (M_{CM}); c) up-climb milled (M_{UCM})

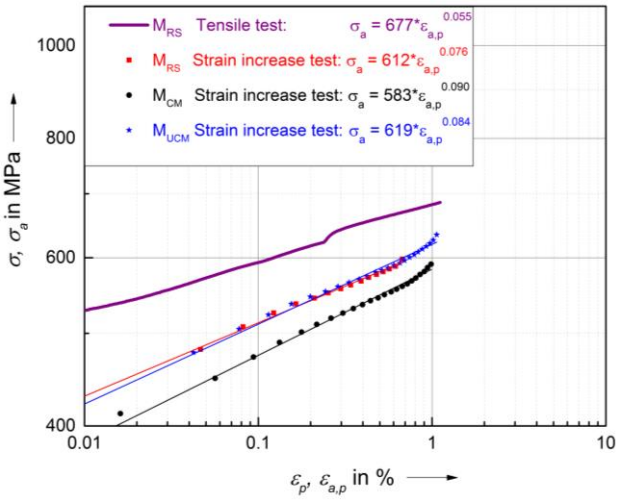

Fig. 8. Cyclic and monotonic stress-strain curves

Fig. 8 compares the monotonic stress-strain and cyclic stress-strain (CSS) curve estimated from strain increase tests (Fig. 7) and tensile tests (Fig. 6). For the CSS curve the average values of stress amplitude σ_a and plastic strain amplitude $\varepsilon_{a,p}$ of the last 25 cycles of each step of the strain increase tests are plotted against the values of stress σ and plastic strain ε_p of a tensile test, with loading direction transverse to the rolling direction. For every morphology, the stress level of cyclic loading was significantly lower than the stress level of monotonic loading. The cyclic yield strength is defined hereafter as the stress level at a plastic strain amplitude of $\varepsilon_{a,p}$ = 0.2 % to a comparable value to $R_{p0.2}$. At $\varepsilon_{a,p}$ = 0.2 % the cyclic yield strength was 505 MPa for morphology M_{CM} and 563 MPa for the morphologies M_{RS} and M_{UCM} respectively. Thus, the HSD® 600 steel softened due to cyclic loading. Therefore, a cyclic softening is also expected in LCF regime for single step tests. In addition, the stress levels of M_{RS} and M_{UCM} are almost congruent while M_{CM} shows a parallel, but slightly lower development of σ_a during the strain increase test.

3.3 Single step tests

Single step tests for all three surface morphologies at four different total strain amplitudes $\varepsilon_{a,t}$ = 0.4 %, 0.6 %, 1.0 % and 1.4 % were performed (Fig. 9). The results confirmed the cyclic deformation behavior shown by strain increase tests. With increasing total strain amplitude, the initial cyclic hardening became more pronounced. At total strain amplitudes of $\varepsilon_{a,t}$ = 1.0 % and $\varepsilon_{a,t}$ = 1.4 % cyclic hardening occurred within the first 8 or 10 cycles respectively. At total strain amplitudes of $\varepsilon_{a,t}$ = 0.6 % and $\varepsilon_{a,t}$ = 0.4 % the initial cyclic hardening occurred just within the first three cycles and was barely observed for M_{RS}. Furthermore for all three morphologies, the cyclic hardening merged to cyclic softening with increasing cycle number. At higher total strain amplitudes of $\varepsilon_{a,t}$ = 1.0 % and $\varepsilon_{a,t}$ = 1.4 % this cyclic softening remained until fracture. At lower total strain amplitudes of $\varepsilon_{a,t}$ = 0.6 % and $\varepsilon_{a,t}$ = 0.4 % the cyclic softening merged into saturation state before fracture, which became more pronounced with decreasing total strain amplitude.

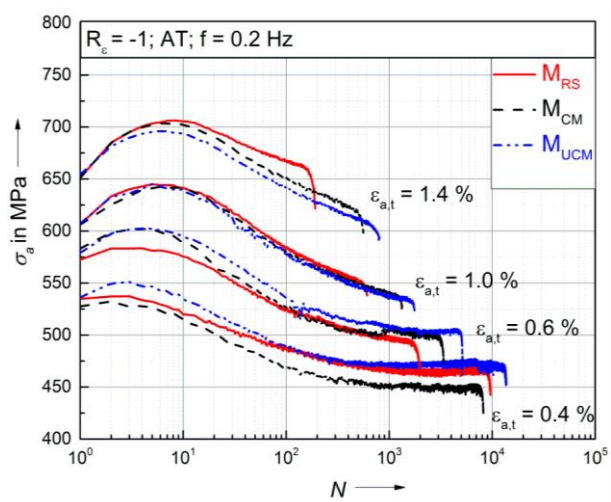

Fig. 9. Development of stress amplitude versus number of load cycles of the three investigated surface morphologies

As well as in strain increase tests, the morphology M_{RS} showed deformation induced phase transformation from γ-austenite to α'-martensite. Fig. 10 shows the cycle and load dependent development of α'-martensite. The

α'-martensite volume fraction increased continuously with the increasing number of cycles and reached higher values at higher loading amplitudes. Maximum values of α´-martensite in the range 0.51 FE-% < ξ < 1.33 FE-% were observed at specimen failure. The development of α'-martensite is comparable to the results from fatigue tests of metastable austenitic Cr-Ni stainless steel [9, 12].

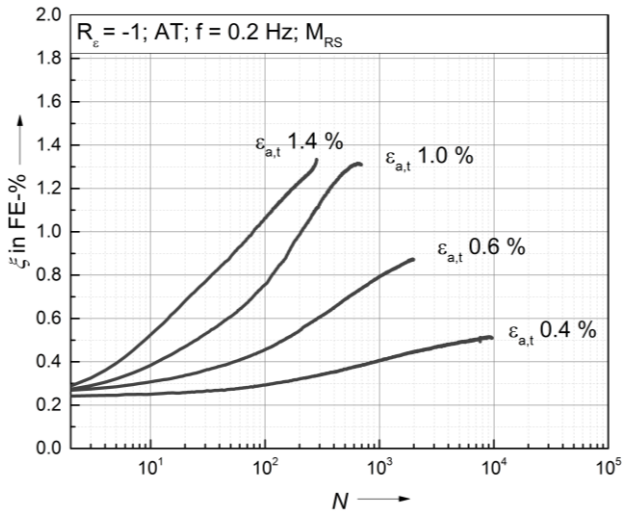

Fig. 10. Development of cyclic deformation induced α'-martensite (ξ) in M_{RS} during fatigue tests

The influence of the different surface morphologies on fatigue life in LCF regime is summarized in Fig. 11 by the total-strain based S-N curve.

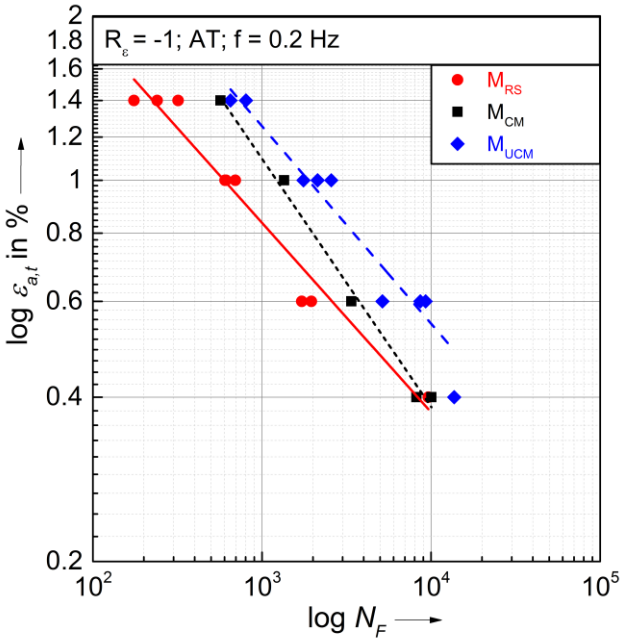

Fig. 11. S-N curve of specimens with different surface morphologies

The specimen with the highest lifetime at all loading amplitudes were M_{UCM}, while the specimen with morphology M_{RS} had the lowest lifetime. However at $\varepsilon_{a,t}$ = 0.4 % M_{RS} achieved a higher number of cycles to failure than M_{CM}, although the surface roughness was eight times higher (see. Fig. 4 and table 3). Therefore, the positive influence of α'-martensite formation on the surface during fatigue loading becomes noticeable but only at low total strain amplitude. For a better understanding of the influence of the surface morphologies at lower load amplitude further high cycle fatigue (HCF) and very high cycle fatigue (VHCF) tests will need to be performed.

4 Conclusion

The cyclic deformation behavior in the LCF regime as well as the monotonic deformation behavior of the TWIP HSD® 600 steel with three different surface morphologies were investigated by strain increase tests, single step tests and tensile tests respectively. The morphologies were as-received with rolling skin (M_{RS}), climb milled (M_{CM}) and up-climb milled (M_{UCM}). Machining was performed in the gauge length respectively. The three morphologies varied in initial residual stresses, roughness and initial phase composition. M_{RS} showed a significant amount of α'-martensite of 32 wt % while the morphologies M_{CM} and M_{UCM} were fully austenitic before loading. The roughest surface occurred in M_{RS} condition with a value of R_z of 6.17 µm, while the morphology M_{CM} showed a value of R_z of 0.75 and M_{UCM} of 1.18 µm. Every morphology had residual compressive stress before loading but the amount varied from -100 MPa for M_{RS} to -600 MPa for M_{CM} and -800 MPa for M_{UCM} respectively.

The strain increase tests as well as the single step tests showed a dependence of the deformation behavior on the applied total strain amplitude. With increasing strain amplitude, an initial cyclic hardening occurred and the higher the applied total strain amplitude the more pronounced was the initial cyclic hardening. This cyclic hardening merged into cyclic softening until fracture or, at lower total strain amplitudes, was followed by cyclic saturation. Nevertheless, the cyclic yield strength was significantly lower than the monotonic yield strength for all three surface morphologies.

Although the morphology M_{RS} had an initial amount of 32 wt % α'-martensite on its surface and showed further α'-martensite formation induced by cyclic loading, it led to the shortest lifetime due to its significantly higher roughness. The machined surfaces were comparable in their achieved lifetimes, but the climb milled morphology showed slightly lower stress levels at cyclic loading.

The authors gratefully acknowledge financial support from Deutsche Forschungsgemeinschaft (DFG) within the Collaborative Research Center (CRC) 926, the chair MT&S of Prof. Seewig for confocal microscopy and the use of µSoft explorer, and Salzgitter AG for providing the HSD® 600 steel.

References

1. G. Frommeyer, U. Brüx, P. Neumann, ISIJ Int. **43**, 438–446 (2003)
2. I. Gutierrez-Urrutia, D. Raabe, Scr. Mater. **66**, 992–996 (2012)
3. M. W. Klein, R. Skorupski, M. Smaga, T. Beck, Engineering Transaction, 69–75 (2017)
4. A. Saeed-Akbari, A. Schwedt, W. Bleck, Scr. Mater. **66** 1024–1029 (2012)
5. A. S. Hamada, L. P. Karjalainen, J. Puustinen, Mater. Sci. Eng., A **517**, 68–77 (2009)
6. C. W. Shao, P. Zhang, R. Liu, Z. J. Zhang, J. C. Pang, Z. F. Zhang, Acta Mater. **103**, 781–795 (2016)
7. P. Guo, L. Qian, J. Meng, F. Zhang, L. Li, Mater. Sci. Eng., A, **584**, 133–142 (2013)
8. R. Skorupski, M. Smaga, D. Eifler, Adv. Mater. Res. **891-892**, 464–469 (2014)
9. M. Smaga, R. Skorupski, D. Eifler, T. Beck, J. Mater. Res. **39**, 1–9 (2017)
10. W. Z. Zhuang, G. R. Halford, Int. J. Fatigue **23**, 31–37 (2001)
11. H. Knobbe, P. Starke, S. Hereñú, H.-J. Christ, D. Eifler, Int. J. Fatigue **80**, 81–89 (2015)
12. M. Smaga, F. Walther, D. Eifler, Mater. Sci. Eng., A **483-484**, 394–397 (2008)